Analysing the modifications of carbon black and other fillers after pyrolysis of model tyres

Petros Kasaira Mubari, Elsa Weiss-Hortala, Marc Monthioux, Sébastien Moyano, Alex Bowles, Geoff Fowler, Ludovic Moulin, Pascal Puech

Analysing the modifications of carbon black and other fillers after pyrolysis of model tyres

Petros Kasaira Mubari [a,b], Elsa Weiss-Hortala [b,c], Marc Monthioux [a], Sébastien Moyano [a], Alex Bowles [d], Geoff Fowler [d], Ludovic Moulin [e], Pascal Puech [a,*]

[a] CEMES, UPR8011-CNRS, Université de Toulouse, 29 rue Jeanne Marvig, 31055 Toulouse CEDEX 04, France
[b] Centre RAPSODEE, UMR CNRS 5302, Mines Albi, Université de Toulouse, Campus Jarlard, 81013 Albi Cedex 09, France
[c] Institute of Multidisciplinary Research for Advanced Materials (IMRAM), Tohoku University, Sendai, Japan
[d] Department of Civil and Environmental Engineering, Imperial College London, SW7 2AZ, UK
[e] Alpha Carbone, 4 rue Jules Védrines, 31031, Toulouse, France

A B S T R A C T

Carbon blacks (CBs) that are used as fillers to reinforce rubber contribute to tyre recycling issues. Although recovered carbon black (rCB) produced from the thermoconversion of waste tyres has poor reinforcing abilities in non-polar rubbers, the exact origin of the difference between rCBs and CBs is not elucidated. The characteristics of the rCBs produced from the steam pyrolysis of model laboratory-reinforced rubbers, with or without silica added, were analysed and compared to the pristine CB. X-Ray Diffraction revealed that the quantity of unorganised carbon in the rCB increased by about 25% after pyrolysis, revealing the occurrence of carbonaceous deposits originating from rubber carbonisation. They affected the filler texture, and part of the ultramicroporosity (*i.e.*, pores within the diameter range 0.34–0.76 nm), which had a three-fold decrease in the rCB sample. The recovered fillers, with and without silica, had more oxygenated functional groups than the CB. The dispersibility and stability of the colloidal suspensions were affected by the increased surface oxygen functional groups. Reductive hydrogenation was utilised to remove the excess oxygen allowing an improved understanding of the rCBs. This is a promising method to maximise material reutilisation in the circular value chain of tyres.

1. Introduction

Tyres are composite products comprising formulations based on rubber, textile fibres, and metallic cables. The tread ensures contact with the rad and is mainly made up of elastomers and fillers including carbon blacks (CBs) and silica [57]. Fillers added to rubber vulcanisates improve strength, flexibility, fatigue resistance, abrasion resistance, and other properties [45,49]. For readers non-familiar with CBs, a detailed description of the material and its manufacture is given in the supplementary Information (SI, sections 1 and 2) of this manuscript. The combined use of CB and silica as a hybrid filler takes the advantages of both fillers in tyre treads. The synergistic effect results in improved tyre wet traction and rolling resistance [64]. Waste tyres can be valorised by thermochemically separating the components of a tyre, facilitating consecutive material and energy recovery [50]. Thermal treatment of waste tyres by pyrolysis is conducted in an oxygen-free atmosphere, using a wide range of equipment, such as vacuum pyrolysis, fixed, fluidised beds, spouted, augers, and plasma reactors [6,12,24,28,34].

The thermoconversion methods are utilised to process waste tyres into tyre pyrolysis oil, tyre pyrolysis gas, and recovered fillers in the form of recovered carbon black (rCB) and recovered silica [19,26,27,31,32,35,38,57,59]. The solid component obtained after the thermoconversion of rubber formulations is a mixture containing rCB and recovered silica (if present), and ashes (Zn and S compounds) from vulcanisation reactions. CB is composed of (i) primary particles, (ii) aggregates (clusters with chemical interactions), and (iii) agglomerates (with physical interactions). The aggregate is the basic dispersive unit that drives the dispersibility of the material in the rubber and provides

reinforcing properties.

There is a growing consensus that rCB has the potential to be used as reinforcing filler in rubber formulations as an alternative to pristine CB, thereby improving the life cycle of the petroleum-based material through increased circularity [10]. Fillers must be effectively dispersed in rubber vulcanisates to improve their mechanical properties, but currently rCBs do not meet this criterion, leading to poor reinforcement capabilities [4,36,65]. The major conclusions that were drawn to explain the discrepancies between CBs and rCBs were:

- rCBs are very heterogeneous, and they vary in primary particle size distribution depending on the waste tyres used as feedstock during thermoconversion. They can be described as a mixture of various commercial rCBs, ash, and some carbonaceous deposits [7,10,46,57,58]. To improve rCB performance, research work has been conducted to reduce the ash content in rCBs by leaching [8], the demineralisation, however, resulted in an increase in acidic functional groups. For a model rubber formulation producing rCB with little ash content, filler dispersibility did not improve and the resulting reinforcement improvements were thus minimal [38].
- Thermoconversion increases the amount of oxygen and volatile matter in rCB in comparison to pristine CB [12,13] but its nature and impact on the filler properties are not explained in detail.

The physicochemical complexity of rCB results in difficulties in outlining the impact of the ash content, carbonaceous deposits, and aggregate morphology on the overall properties of the rCBs, especially their dispersibility. It is therefore necessary to establish the origin of the contrasted behaviours of rCB compared to pristine CB by analysing the physicochemical differences of both materials.

It has been suggested that superheated steam reduces residual volatile matter in rCB, as steam diffuses into solid particle pores even at lower temperatures, eliminating post-treatment compared to traditional pyrolysis [27,34]. Here, a comparative multiscale characterisation scheme is utilised for rCB and rCB-SiO_2 (both obtained from the thermoconversion of model rubber formulations) and pristine CB, looking into aspects such as the structural, nanotextural, textural, and chemical properties. Potential findings may therefore be used to apply appropriate modification and post-treatment methodologies on the rCB to improve its dispersibility in non-polar rubbers.

2. Experimental details

2.1. Materials

2.1.1. Rubber/filler composites and components

rCBs were produced from two model rubber formulations representative of the tyre tread. The first comprised of 31.91 wt% CB (N330 grade supplied by Corax) and the other comprised a hybrid filler in the form of a physical mixture of 15.75 wt% CB and 15.75 wt% ULTRASIL® VN 3 silica supplied by Evonik Industries. The effect of adding silica was studied because current tyres contain a proportion of silica which is increasing. Both fillers (CB, and the physical mixture of CB + silica) were blended in an elastomer matrix of SBR/NR (styrene butadiene rubber/natural rubber). The rubber compound also included the plasticizing oil Plaxolene® MS and a standard vulcanisation system (see section 3 in SI). Bis[3-(triethoxysilyl) propyl] tetrasulfide (TESPT) was added as a coupling agent between the silica and the elastomer. Two rubber protectors were also introduced as detailed in Table 1. The blend was produced in a 3.3 L mixer at a rotor speed of 40 rpm by Elanova.

These formulations were thermally treated using a hybrid pyrolysis process to recover the filler components from the rubber formulation. The rubbers were heated at a constant heating rate of 5 °C/min to 550 °C under a 5 L/min flowrate for both N_2 and steam, at atmospheric pressure. A 90-min isotherm was then held, after which steam introduction is stopped and the system was cooled down to the ambient temperature at a steady rate of 5 °C/min under N_2. The pyrolysis conditions used (heating rate of 5 °C/min at 550 °C) ensure complete rubber degradation [1,11,28,47].

Table 1
Model rubber formulations without and with silica.

Role	Ingredients	Without Silica (wt%)	With Silica (wt%)
Elastomer matrix	S-SBR BUNA VSL 4526–0 HM	36.47	36
	NR 10CV60	9.12	9
Fillers	Silica VN3	0	15.8
	Corax N330	31.91	15.8
Aromatic plasticiser	Plaxolene MS	15.95	15.8
Vulcanisation activators	ZnO Neige B	1.37	1.35
	Stearic acid	0.68	0.68
Protectors	6PPD	0.68	0.68
	Antilux 500	0.68	0.68
Coupling agent	Silane Si69	0	1.26
Vulcanisation Accelerators	Sulphur	1.14	1.13
	CBS 80	0.85	0.84
	DPG 80	1.14	1.13
	Total	100	100

Two types of fillers were recovered, rCB corresponding to the first rubber formulation and recovered carbon black/silica hybrid filler (rCB-SiO_2) corresponding to the second formulation. The yields of recovered fillers were 34.7 wt% and 34.1 wt% for rCB and rCB-SiO_2, respectively. These yields are consistent with the literature [57] since this is inclusive of the recovered filler, ashes and carbonaceous residues. All the samples were subjected to mechanical grinding prior to the tests, analyses were thus performed on fine powders.

2.1.2. Post-treatment of recovered carbon blacks: reduction with hydrogen gas

An initial approach to correct the chemical composition of the rCB surface consisted of reducing the surface oxygen functional groups using a flow of hydrogen gas in a continuous flow tubular reactor under two different conditions, at 400 °C for 1 h and 550 °C for 2 h, both at a gas flowrate of 200 mL/min at atmospheric pressure. The resulting material was designated as rCB-R.

2.2. Characterisation of the fillers

The characterisation of rCBs using methods derived from American Society for Testing and Materials (ASTM) standards developed for pristine CBs, does not reveal the modifications induced by the thermochemical process that affect filler dispersibility [38]. Focus is therefore placed upon the changes that arise from the thermoconversion process on the filler characteristics by employing techniques described below.

2.2.1. X-ray diffraction (XRD)

XRD diffraction patterns of the fillers were recorded on a Bruker RX-D8 Advance ECO X-ray diffractometer with a non-monochromated Cu K_α radiation source (average $\lambda = 1.5406$ Å). The diffractograms were acquired at 0.02° s^{-1} in the 2θ range 15–70°. The different phases present were analysed with the DIFFRAC.SUITE EVA software from Bruker.

2.2.2. Energy dispersive X-ray spectroscopy (EDX)

EDX mapping on the rCB-SiO_2 sample was performed using a Philips CM20FEG operated at 200 kV for determining the elemental distribution.

2.2.3. Gas sorption analysis

Gas sorption analysis was conducted on a Micromeritics 3Flex adsorption analyser. A standard procedure was followed: sample degassed at 300 °C for 5 h, N_2 and Ar adsorption was carried out at 77 K,

CO_2 adsorption isotherms were acquired at 273 K. To treat the data, Brunauer–Emmett–Teller (BET) method was applied to adsorption in the relative pressure (P/P_0) range 0.05–0.3, micropore volume was determined *via* the non-linear density functional theory (NLDFT). Each sample was analysed in duplicate, with the mean presented as the best estimator. Adsorption designates retaining gas molecule on the pore surface. Absorption designates retaining gas molecules in the pore volume. The Barrett, Joyner, and Halenda (BJH) method which applies to mesoporous or macroporous materials was used for calculating pore size distributions by employing the Kelvin model of pore filling on experimental isotherms (desorption branch between P/Po = 0.35–0.99).

2.2.4. Thermogravimetric – differential thermal analysis (TGA-DTA)

A Setaram TGA-DTA 92 was used to evaluate the thermal stability of the fillers. The samples (weight ~ 15 mg) were heated from 30 to 1200 °C at a rate of 10 °C /min under a 3 L/h N_2 flowrate.

2.2.5. Temperature programmed desorption coupled with micro gas-chromatography (TPD-μGC)

The sample was purged by flushing with nitrogen at 33 mL/min for 20 min, then the sample was subjected to continuous heating under helium at 10 °C/min from 30 to 1000 °C. CO and CO_2 gas production was monitored by μ-GC (My-GC SRA Instruments). The temperature at which the surface oxygen functional groups decompose to give the carbon oxides makes it possible to determine their nature [16,20,52]. Hence it is more about defunctionalisation than gas desorption, in that case.

2.3. Dispersibility studies

The colloidal stability of the fillers: CB, rCB, rCB-SiO_2, and rCB-R in different solvents (acetone, ethanol, *N*-methyl-2-pyrrolidone (NMP), binary mixture of ethanol + water, and water) was assessed. Selected physical properties of the solvents are listed in Table 2.

A substance with a high relative permittivity is easily polarised. A polar solvent will stabilise or (disperse) polar particles by generating stabilising connections with the colloids that outweigh particle-particle interactions (relative permittivity: $\boldsymbol{\varepsilon_r} > 15$). The surface tension of a liquid influences powder wettability and eventual dispersibility depending on the powder hydrophilic properties.

The stability of the colloidal dispersions (0.05 mg/mL) loaded in optical glass cuvettes was determined by measuring the transmission of light from a 10 mW argon laser of wavelength 528 nm (1 mm spot diameter). The intensities of the transmitted light at time $t = 0$ h (immediately after preparation) and $t = 16$ h (left without any displacement) were measured. Light transmission was converted into absorbance, large absorbance values are synonymous with stable systems.

3. Results and discussion

3.1. Structure and nanotexture evaluation of the fillers

The structure and nanotexture associated with CB, rCB and rCB-SiO_2 fillers was investigated with XRD (Fig. 1). CB exhibits a turbostratic

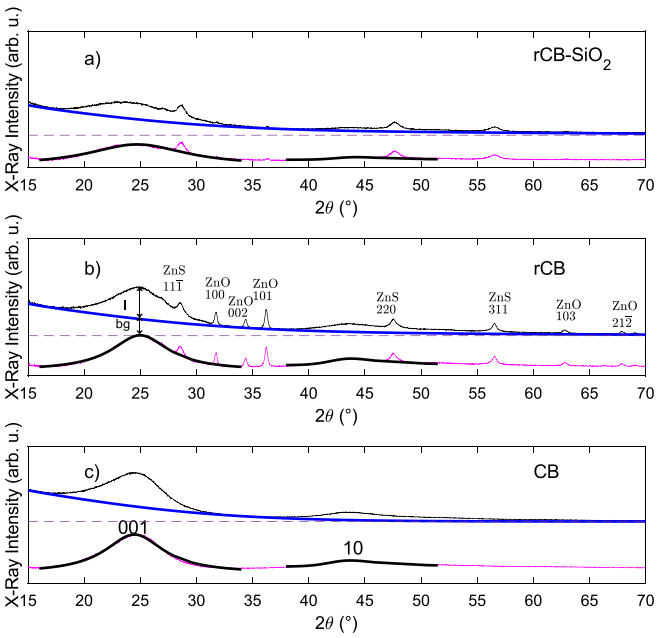

Fig. 1. XRD profiles before and after background removal for (a) rCB-SiO_2; (b) rCB and (c) CB. The upper part represents the raw diffractogram (black line) and the baseline considered (blue line); the lower part (magenta line) is the XRD profile after removing the background by employing continually decreasing functions considering the X-ray scattering factor and the fitting by parametrised functions (bold black lines).

structure, *i.e.*, 2D instead of 3D as in graphite, and of course the recovered CBs remain the same, as evidenced by the absence of 3D-characteristic peaks such as *101*. The peaks related to the turbostratic carbon crystallites are indexed as *001* ($2\theta \approx 25°$, often named *002* in the literature in reference to graphite, and corresponding to the average intergraphene distance d_{001}, hence along *z* direction), and *10* ($2\theta \approx 44°$, arising from the in-plane periodicity). The average crystallite diameter in the basal plane (L_a) was calculated from the *10* peak, based on the method proposed by Puech et al. [44], whilst L_c, the average thickness perpendicular to the basal plane was derived from the Scherrer equation applied to the *001* peak.

According to (Table 3), the characteristics of the carbon crystallites (d_{001}, L_a, L_c) in CB are consistent with that from the literature [15], and do not change after thermoconversion. The results also attest that L_c primarily indicates the average stacking of three carbon layers per crystallite.

When compared to the other samples, rCB-SiO_2 exhibits a broader *001* peak due to the overlapping of the amorphous silica peak at around $2\theta \approx 22°$ with the *001* peak [3]. In addition to amorphous silica, peaks occur related to additional crystallized phases linked to impurities in the recycled fillers. These impurities were identified as ZnO and ZnS, with an average crystallite size of ~10 nm as obtained using the Scherrer equation (with K = 0.89). ZnS originates from ZnO (Table 1) through the curing reaction with sulphur [14,42,53]. In the rCB sample, there is a

Table 2
The selected physical parameters of the solvents at 20 °C.

Solvent	Acetone	Ethanol	NMP	Water/Ethanol 50:50 (v/v)	Water
Relative permittivity ε_r	21.3 [22]	25.1 [60]	32.6 [40]	55.0 [60]	80.4 [60]
Surface tension in air (mN/m)	23.0 [23]	22.3 [2]	41.0 [25]	26.0 [29]	72.7 [56]

Table 3
XRD parameters for the different types of Bs.

Extracted parameters	Material		
	CB	rCB	rCB-SiO_2
L_c (nm) from *001*	1.20	1.20	1.20
L_a (nm) from *10*	2.40	2.33	2.40
d_{001} (Å)	3.64	3.56	3.60
$a_{C=C}$ (Å)	1.42	1.42	1.42
$\frac{I_{bg}}{I_{001}}$	0.52	0.65	1.16

significant contribution of ZnO to the diffractogram, which is not present in the rCB-SiO_2. The reaction of stearic acid with ZnO to create zinc stearate as a necessary curing activator is widely recognised [37,55]. When silica is incorporated, an ion-exchange side reaction between surface silanol groups and zinc stearate is the most logical explanation for the reduction of ZnO. These reactions deplete the ZnO and regenerates stearic acid, which then consumes more ZnO [9]. A representative transmission electron microscopy (TEM) micrograph together with the EDX elemental mapping showing the spatial relationships between SiO_2 nanoparticles and Zn and S is shown in Fig. S.1 (supplementary information).

To further analyse the diffractograms, the background at lower 2θ angles was investigated. The background of the diffractograms (*bg*) is related to random X-ray scattering arising from the non-organised carbon phase [39,48]. This is roughly proportional to the number of electrons around the atom nucleus. The Compton effect and other scattering sources also contribute to the background. The intensity ratio of the background over the *001* peak, representing unorganised matter *versus* organised carbon, is denoted by I_{bg}/I_{001} (Table 3). This ratio is relatively higher for rCB in comparison with CB. Indeed, the pyrolysis process results in the release of volatile materials as the elastomer degrades, accompanied by the successive formation and accumulation of char-like carbonaceous deposits by polymerisation and polycondensation reactions of hydrocarbon compounds adsorbed on the filler surface [11,36,62]. The carbonaceous deposit increases by about 25% the amount of unorganised carbon ($\left(\frac{X_{rCB}-X_{CB}}{X_{CB}}\right)$, where $X = \left(\frac{I_{BG}}{I_{100}}\right)$). This ratio is even higher for rCB-SiO_2 because of the contribution of the poorly organised silica. There is also evidence of a proportionate increase in carbonaceous deposits in the rCB-SiO_2 sample, considering that this sample was recovered from a formulation having half the CB content.

3.2. Textural properties of the fillers

The nitrogen and argon adsorption/desorption isotherms of CB and rCB are shown in Fig. 2. In both cases, the isotherms are close to type II-(b) isotherms according to the IUPAC classification. The low volume adsorbed at lower relative pressures indicates that the adsorbents have very low pore volumes and specific surface areas of micropores (*i.e.,* pores with diameters <2 nm). A very slight hysteresis is present at higher relative pressures, so-called H3 hysteresis because it is characteristic of aggregates forming adsorbents and is marked by the absence of a saturation plateau [63]. This therefore indicates that there is no sign that the mesopores (if any) have been fully filled [51]. The adsorption volume does not reach saturation when it is close to $P/P_0 = 1$, which might be possible clustering of the adsorbed molecules on the solid surface at preferable active sites [54]. With N_2 sorption, the hysteresis may be due to flexible texture (gas sorption-induced swelling) under the effect of the capillary condensation of N_2. The lack of a well-defined hysteresis in the case of Ar sorption implies that the N_2 sorption induced swelling in the spaces where this phenomenon occurs. The sorbed N_2 volumes were approximately 500 and 450 cm^3/g for CB and rCB respectively. For Ar adsorption (no condensation of argon at 77 K), the volumes were significantly lower (81 and 77 cm^3/g, respectively). This difference between the values obtained using the two gases is due to changes in the sample volume and thus to a combination of adsorption and absorption, with the latter contributing to ≈ 90% of the sorbed volume. Polar groups (phenolic, ketones, carboxylic, ether bridges, *etc.*) also participate in strong specific interactions with the nitrogen quadrupole unlike argon [41]. The lower amount sorbed in the rCB sample suggests that it is less porous than the CB sample. With the mean primary particle diameter of the fillers being in the range of 30 nm, what is referred to as "porosity" are the spaces between the aggregates and agglomerates.

Table 4 summarises the statistics for the pore volume and surface area of the samples from the N_2 and Ar adsorption isotherms in Fig. 2.

BET-SA values from Ar adsorption were 69 and 67 m^2/g for CB and rCB respectively.

The BET surface area for nitrogen adsorption is very similar for CB (79 m^2/g) and rCB (76 m^2/g), with a slight proportion of this surface area being involved in micropores. The average interparticle spacing (pore width) of rCB was slightly smaller (42 nm) than that of CB (48

Table 4
Gas sorption analysis results. BET-SA = BET surface area. μP-SA = micropore surface area, as determined *via* t-Plot analysis. t-PV = total pore volume. Av-PW = average pore width.

	Materials	
	CB	rCB
N_2 Gas sorption results		
BET-SA [m^2/g]	79	76
μP-SA [m^2/g]	4.32	1.69
t-PV [cm^3/g]	0.80	0.60
Av-PW [nm]	48	42
CO_2 gas sorption results		
μP-SA [m^2/g]	42	29

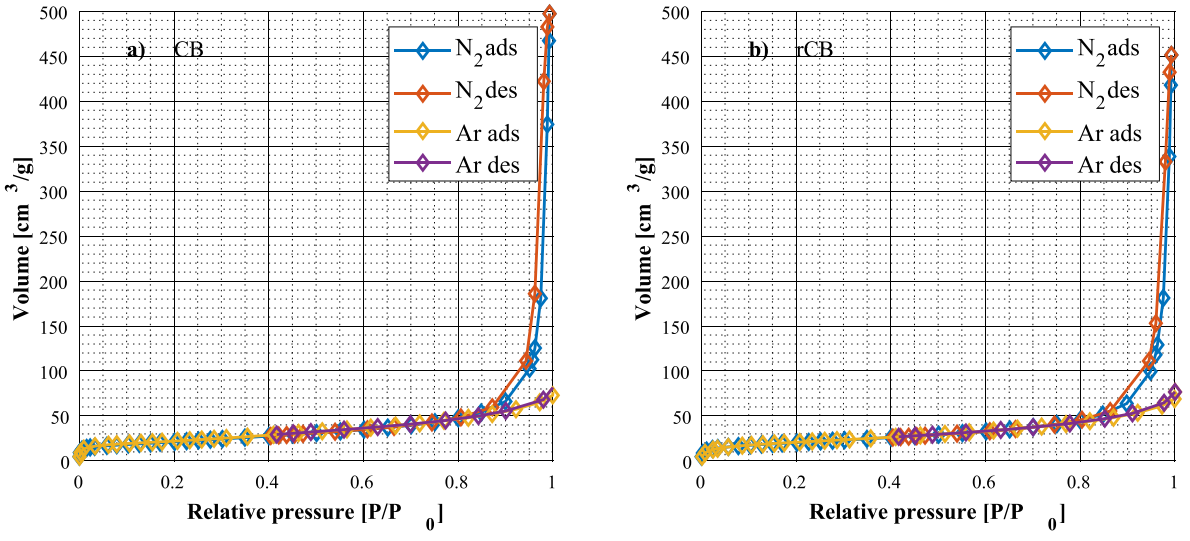

Fig. 2. N_2 and Ar isotherms for the a) CB and b) rCB samples. Each isotherm is split into its adsorption and desorption curves.

nm). The already low microporous surface area (~4.32 m^2/g) in CB is even lower for rCB (~1.69 m^2/g), which may relate to the carbonaceous residue revealed by XRD and deposited on the surface of CB, which partly blocks the access to micropores. Pore size and volume reduction is also a result of nanometric zinc particles which occupy the spaces between agglomerates. The BET surface area measured by argon at 77 K is unreliable because argon at these conditions is below its bulk triple point temperature by 6.5 K, therefore putting the bulk reference state in doubt [54]. As a result, Ar re-sublimates with higher pressures, causing uncertainty regarding the actual area occupied by the Ar atoms.

The narrow micropores (ultra-micropores, *i.e.,* pores smaller than 1 nm in diameter) were assessed *via* processing CO_2 adsorption isotherms which were obtained at 273 K (Fig. 3.a)., as N_2 has a limited diffusion potential in this pore size range. According to Table 4, the CB sample has a higher proportion of ultra-microporous surface area (~ 42 m^2/g) corresponding to pores in the range 0.3–0.8 nm than rCB (~29 m^2/g).

The CB sample had three peaks at 0.43 nm, 0.56 nm, and 0.67 nm on its pore size distribution (Fig. 3.b) whilst rCB has four (0.43, 0.52, 0.61, 0.74 nm), which are well less developed. In general, the successive peaks in the pore size distribution of both samples have a uniform spacing of ~0.11 nm which indicates similar molecular level surface roughness. These ultra-micropores are interstices between crystallites, intrinsic to their poor alignment. The modification of the distribution in rCB is indicative of carbonaceous deposits on the interstices between crystallites and surface functionalisation of the graphene sheets at the edges on the primary-particle surface during thermoconversion. The apparent quantity of the micropores is thereby decreased in rCB due to the partial blocking and limiting access to the interstices.

3.3. Thermal stability of the fillers

The superficial additional carbon phase was probed by thermal stability methods. The thermograms of the fillers shown in Fig. 4 demonstrate that CB is more stable than the recycled fillers. CB and rCB have the same decomposition profile whilst that of rCB-SiO_2 is suppressed because SiO_2 has an inhibiting effect on decomposition reactions.

Two distinct weight-loss patterns were observed in all the samples. The part up to a temperature of 180 °C was due to absorbed moisture and volatiles. The rCB-SiO_2 sample had the lowest moisture content due to the silica component which turned hydrophobic with the TESPT coupling agent. The other two fillers (CB and rCB) had an identical moisture content. When the temperature was raised further (>180 °C), the second weight-loss was steady for all the samples between 180 and

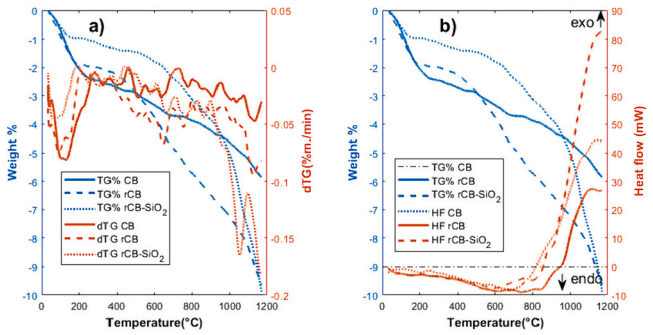

Fig. 4. Thermograms (TG, blue lines) of the pristine and recycled fillers, associated to (a) the derivative of the TGs (dTG, red lines), (b) the heat flow (HF, red lines).

520 °C, due to the desorption of gases and the decomposition of functional groups from the material surface. CB had the greatest mass loss in this region as some of the decomposition (elimination of carboxyl groups) had already taken place in the recycled materials during the rubber-composite thermoconversion, since the highest heating temperature was 550 °C. In this region, rCB-SiO_2 had a similar mass loss as CB and rCB up to ~450 °C (as the TG slopes are similar), despite it contains half the amount of CB. Impurities including sulphur, zinc sulphide, and zinc oxide in both the recycled materials make them multi-component systems thereby imposing different decomposition kinetics of the materials after ~650 °C.

The TGA-dTG thermograms show the final phase of mass loss from 550 °C up to 1200 °C. For CB and rCB, the successive peaks of the dTG curves do not revert to the baseline, so the decomposition steps are inseparable from the preceding ones. This region shows that globally, the pristine material (CB) is the most thermally stable and has smaller weight-loss gradient than rCB (and rCB-SiO_2). Weight loss within the region of 600 to 950 °C is similar for rCB and rCB-SiO_2. This can be related to the secondary carbonisation of the carbonaceous deposits formed during thermolysis, which generates a weight loss corresponding to the elimination of more stable functional groups (ether bridges, ketone) since the material becomes more and more polyaromatic.

3.4. Characterisation of oxygen surface functional groups

The TPD-μGC data in Table 5 quantifies the gases after integration of the areas under the curves of Fig. 5, which illustrates how carbon

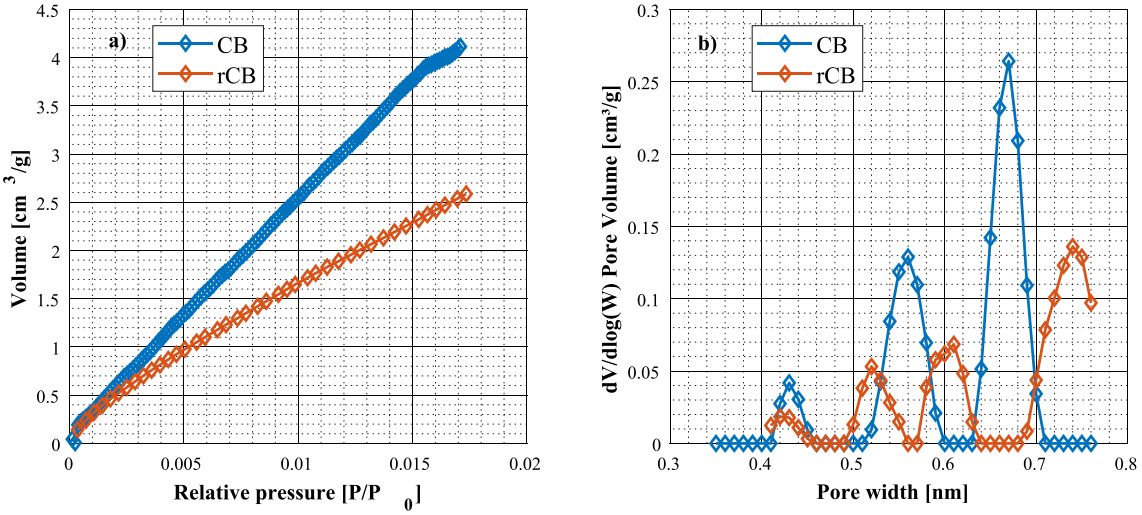

Fig. 3. a) CO_2 adsorption isotherms, and b) the change in pore volume, as a function of pore width for the two samples, as determined *via* the application of the NLDFT theory to CO_2 adsorption data at 273 K.

Table 5
Amounts of gases released from the fillers, per gram of material.

Sample	Released gas (mmol/g)			
	CO	CO_2	Total	CO: CO_2
CB	1.8	1.1	2.8	1.6
rCB	3.9	1.4	5.3	2.8
rCB-SiO_2	2.8	0.7	3.5	4.0

monoxide and carbon dioxide gases evolve as a result of the decomposition of oxygen surface functional groups when the fillers were heated up to 1000 °C.

Both recovered fillers release slightly more CO_2 and much higher amounts of CO than CB, and even more if considered per gram of carbon instead of per gram of material, thereby providing evidence of more oxygenated groups. The latter are due to a combination of oxygen functionalities grafted onto rCB and from the carbonaceous deposits resulting from the carbonisation of the rubber, during thermoconversion. The carbothermic reduction of ZnO (at 1000 °C) [5], which occurs for both recovered fillers may also contribute, although limitedly, to the evolved gas.

The bottom graph in Fig. 5 shows that CO_2 evolution in CB and rCB starts in a similar way, however more gas released at around 400 °C for CB. There are two "peaks" of higher CO_2 production for rCB in the range 180–550 °C and then from 600 to 1000 °C. During the evolution of CO (top graph in Fig. 5), the curves sort of resemble each other with some differences at the extremities (and major differences in the amount of CO released in the 700–1000 °C range).

The evolution of CO_2 is first due to the decomposition of the less stable acidic (carboxylic) functional groups, as well as anhydride and lactone groups [33,52,66]. At higher temperatures (from ~40 min/450 °C), more stable basic and neutral groups such as phenols, carbonyls, quinones, and pyrones decompose, resulting in the evolution of CO [33,52,66]. Both CO and CO_2 are produced when anhydride groups decompose during a two-step reaction at a ratio of 1:1 [17]. The decomposition of the signal into multiple fits using Gaussian functions allowed assigning the functional groups, and is justified by the normal distribution of each functional group. Fig. S.2 (supplementary information) depicts how the signal was fitted. The quantified functional groups for all three samples are illustrated in Fig. 6.

Weak acids in the form of phenols are the most prominent functional group associated with the rCB filler. The increased concentration of phenols during thermoconversion of the compounded rubber is almost five-fold in rCB and two-fold in rCB-SiO_2. There is also a significant but lower quantity of carbonyls and quinones, two times more in rCB and three times more in rCB-SiO_2 in comparison to CB. There is a slightly higher number of pyrones in CB. This is accounted for by the dehydration of some neighbouring phenolic and carboxyl, or carbonyl groups during heating in TPD, thereby producing new lactones. In the rCB sample, these dehydration reactions are partially inhibited. The CO evolution at 1000 °C in the rCB-SiO_2 sample is a result of a combination of the decomposition of pyrones and reduction of some of the silica surface. The TESPT-coupling agent is strongly bonded to the surface of amorphous silica and allows prediction of covalent bonds to have occurred [21]. It has been established that carbothermal reduction of silica usually starts at temperatures above 1200 °C; therefore, it is reasonable to propose that evolved CO can only be a result of the decomposition of the TESPT and oxygenated groups.

3.5. *Colloidal dispersion and stability*

Figure 7 outlines the colloidal stability of the microscopically dispersed CB, rCB, and rCB-R (after H_2 reduction) in different solvents, as characterised by their relative permittivity and surface tension.

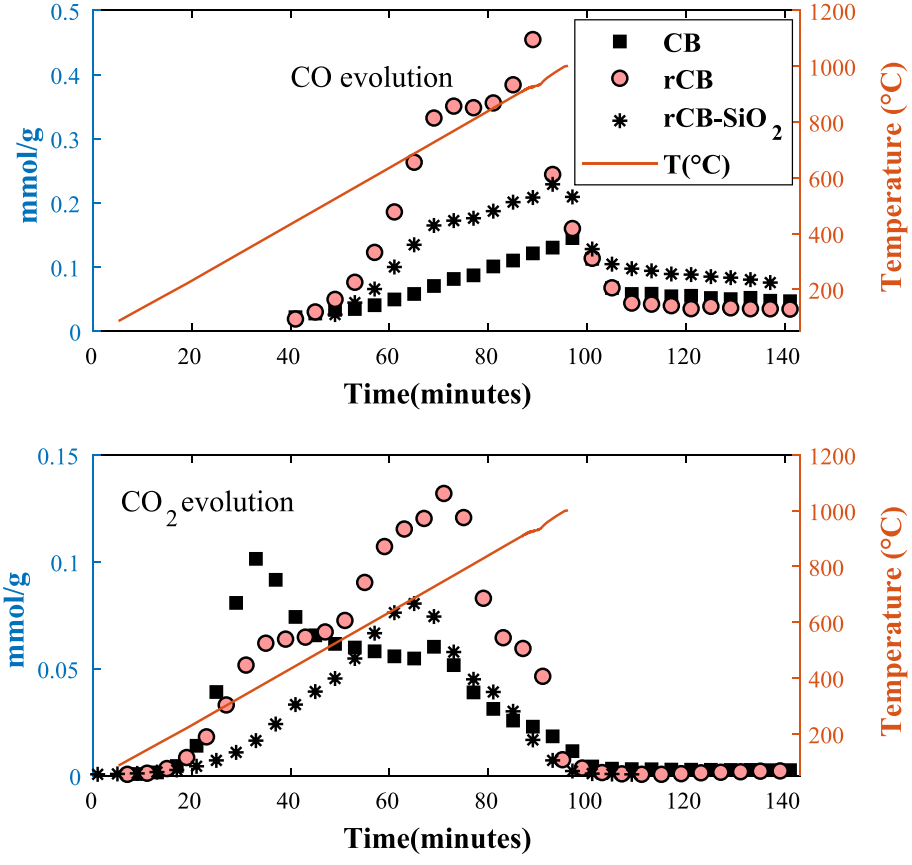

Fig. 5. TPD-μGC profiles of CO_2 (bottom) and CO (top) evolution in function of time and temperature.

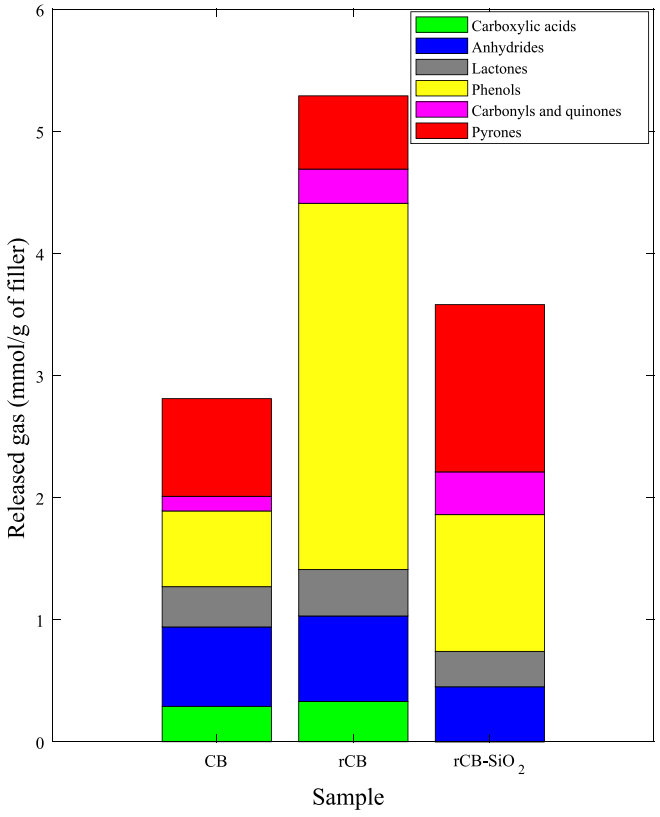

Fig. 6. Distribution and composition of the oxygenated functional groups in mmol/g of filler sample.

Table 6 compares the rCB-SiO_2 colloidal system to that of CB and rCB to investigate the effect of silica and the TESPT coupling agent on the colloidal properties of the recovered filler.

The mass attenuation coefficients for carbon black and SiO_2 are 7.70 × 10^{-6} [43] and 0.55 × 10^{-6} m^2/g [30,61] respectively. From the values of the attenuation coefficients, it is evident that the absorbance of silica is negligible in comparison to that of carbon black. Therefore, in the rCB-SiO_2 sample, the absorbance values therein obtained are mostly due to the rCB content and the carbonaceous residue.

Table 6
Light absorption characteristics of CB, rCB and rCB-SiO_2 in selected solvents.

Solvent	Light absorbance by sample					
	CB		rCB		rCB-SiO_2	
	t = 0 h	t = 16 h	*t* = 0 h	t = 16 h	t = 0 h	t = 16 h
water	0.65	0.37	1.37	1.32	1.03	0.99
Water-ethanol	2.69	2.60	1.75	1.68	1.96	1.83
Ethanol	3.03	2.98	1.95	1.90	2.28	2.25

CB exhibits a poor dispersion in water due to its hydrophobic nature. Dispersion is significantly improved in NMP (Fig. 7), then increases modestly in the equivolume water/ethanol mixture, followed by ethanol and then acetone. In the water/ethanol mixture, the CB dispersion is almost identical as in ethanol, indicating that the ethanol veneers the dispersible units which then disperse in water. As expected, rCB was more dispersible in water than CB by a factor of about 3 corresponding to the five-fold increase in phenols in rCB as well as other functional groups. Hydration repulsive forces are very dominant in rCB, these forces have a stabilising effect against particle agglomeration and sedimentation [18]. rCB-SiO_2 (Table 6) has the same trend as rCB, however the values are not proportionate considering the carbon content, this can be understood by additional functional groups in the former, due to the prior coupling of silica with TESPT. The dispersion of rCB is lowest in acetone (less polar solvent). Excess functional groups in the recovered material increases its surface polarity therefore favouring filler-filler interactions (agglomeration tendencies) in media of little to no polarity through hydrogen bonding. On the contrary, it promotes filler-medium interaction if the polarity of the dispersing medium increases.

Prolonged reduction (rCB-R-550 °C) resulted in attaining the same level of decreased dispersibility as that of the pristine material in water because of a significant loss in surface polarity. The temperature used during the reduction process corresponds to the decomposition of carboxyl and anhydride groups as seen during TPD analyses, hence contributing significantly to the loss of surface polarity.

Although there is an overall tendency to a very slight suspension instability shown by a very slight decrease in absorbance after 16 h, it

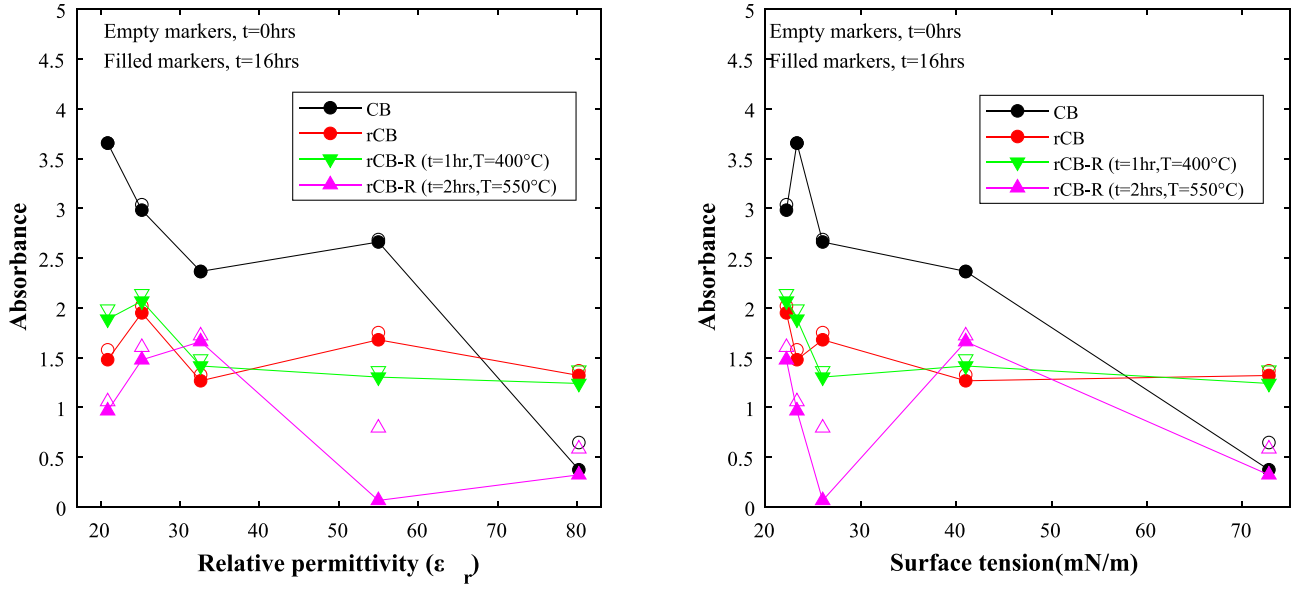

Fig. 7. Dispersibility and stability of the suspensions in various solvents as measured from their absorbance values immediately and after 16 h. From left to right, the various permittivity values correspond to the various solvents, *i.e.*, acetone, ethanol, NMP, water/ethanol, and water, respectively. The various surface tension values correspond to ethanol, acetone, water/ethanol, NMP, and water, respectively (see Table 2).

can be said that all the filler materials were found stable for the conditions tested. Two exceptions, however, showed a significant drop after 16 h, which correspond to (1) the rCB-R-550 °C in water (with a peak for the ethanol/water mixture), and (2) CB in water. This is due to the hydrophobicity and low wettability of these materials in water. The materials have exceedingly low quantities of functional groups translating to low affinity for water molecules, therefore any interaction between them is short-lived resulting in flocculation.

4. Conclusion

The comparative physicochemical characterisation of rCB materials (with or without silica) and pristine CB gave a comprehensive insight into the differences which affect their dispersibilities. Whilst it has been shown that the structural properties of CBs remain the same after thermolysis, ashes and mainly carbonaceous deposits (about 25% more amorphous carbon from X-Ray diffraction) have been demonstrated to alter the texture and surface chemistry of the recovered fillers. If present, silica is also recovered as part of the ash. Due to the vulcanisation, ZnO nanoparticles are present. After thermoconversion, some ZnS nanoparticles were also observed. A significant decrease in microporosity was seen in rCB down to the range of ultra-micropores. The additional oxygen functional groups were considerably higher in both rCB and rCB-SiO_2 in comparison to CB. Among other statements, the surface oxygen functions affect the stability of the colloidal suspension, the recovered fillers were therefore found to be more polar and, consequently, more dispersible in polar media, explaining the reduction in compatibility with non-polar media (such as natural and styrene-butadiene rubbers, for instance). Recycled fillers need to be modified, by reducing the surface oxygen functionalities for the best rubber reinforcement to be achieved. In this regard, reductive annealing under hydrogen is a promising method to maximise material reutilisation in the circular value chain of tyres. In their current state, rCBs can be employed as semi reinforcement materials, or in environmental applications as pollutant adsorbents, and in the production of electrodes for batteries.

Funding

P.K.M. is supported by a Université de Toulouse and Occitanie region scholarship. This study has been partially supported through the EUR grant NanoX n° ANR-17-EURE-0009 in the framework of the "Programme des Investissements d'Avenir". This work was supported by a French government grant managed by the Agence Nationale de la Recherche under the Investissements d'Avenir program, reference ANR-18-EURE-0021.

CRediT authorship contribution statement

Petros-Kasaira Mubari: Writing – review & editing, Writing – original draft, Methodology, Investigation, Formal analysis, Data curation, Conceptualization. **Elsa Weiss:** Writing – review & editing, Validation, Supervision, Resources, Project administration, Methodology, Funding acquisition, Formal analysis, Conceptualization. **Marc Monthioux:** Writing – review & editing, Validation, Formal analysis. **Sébastien Moyano:** Writing – review & editing, Conceptualization. **Alex Bowles:** Writing – review & editing. **Geoff Fowler:** Writing – review & editing. **Ludovic Moulin:** Writing – review & editing. **Pascal Puech:** Writing – review & editing, Validation, Supervision, Resources, Project administration, Methodology, Investigation, Funding acquisition, Formal analysis, Data curation, Conceptualization.

Declaration of competing interest

The authors declare no conflict of interest.

Data availability

Data will be made available on request.

Acknowledgments

D. Neumayer, S. Pinaud, and C. Marcelot from CEMES as well technicians from Rapsodee are acknowledged for technical support.

Appendix A. Supplementary data

Supplementary data to this article can be found online at https://doi.org/10.1016/j.susmat.2024.e00904.

References

[1] O. Al-Hartomy, A. Al-Ghamdi, S. Al Said, N. Dishovsky, M. Mihaylov, M. Ivanov, L. Ljutzkanov, Influence of the carbon-silica reinforcing filler, obtained via pyrolysis of waste 'green' Tyres on the properties of EPDM based composites, KGK Kautsch. Gummi Kunstst. 68 (2015) 56–61.
[2] E. Álvarez, A. Correa, J.M. Correa, E. García-Rosello, J.M. Navaza, Surface tensions of three amyl alcohol + ethanol binary mixtures from (293.15 to 323.15) K, J. Chem. Eng. Data 56 (11) (2011) 4235–4238, https://doi.org/10.1021/je200793z.
[3] R.A. Bakar, R. Yahya, S.N. Gan, Production of high purity amorphous Silica from Rice husk, Proc. Chem. 19 (2016) 189–195, https://doi.org/10.1016/j.proche.2016.03.092.
[4] P. Berki, R. Göbl, J. Karger-Kocsis, Structure and properties of styrene-butadiene rubber (SBR) with pyrolytic and industrial carbon black, Polym. Test. 61 (2017) 404–415, https://doi.org/10.1016/j.polymertesting.2017.05.039.
[5] A. Berman, M. Epstein, The kinetic model for carboreduction of zinc oxide, Le J. Phys. IV 09 (PR3) (1999), https://doi.org/10.1051/jp4:1999349. Pr3–324.
[6] F. Campuzano, N. Cardona-Uribe, A.F. Agudelo, S.M. Sarathy, J.D. Martínez, Pyrolysis of waste tires in a twin-auger reactor using CaO: assessing the physicochemical properties of the derived products, Energy Fuel (2021), https://doi.org/10.1021/acs.energyfuels.1c00890.
[7] N. Cardona, F. Campuzano, M. Betancur, L. Jaramillo, J.D. Martínez, Possibilities of carbon black recovery from waste Tyre pyrolysis to be used as additive in rubber goods -a review, IOP Conf. Ser.: Materi. Sci. Eng. 437 (2018) 012012, https://doi.org/10.1088/1757-899X/437/1/012012.
[8] N. Cardona-Uribe, M. Betancur, J.D. Martínez, Towards the chemical upgrading of the recovered carbon black derived from pyrolysis of end-of-life tires, Sustain. Mater. Technol. 28 (2021) e00287, https://doi.org/10.1016/j.susmat.2021.e00287.
[9] H.M. da Costa, L.L.Y. Visconte, R.C.R. Nunes, C.R.G. Furtado, Rice husk ash filled natural rubber. I. Overall rate constant determination for the vulcanization process from rheometric data, J. Appl. Polym. Sci. 87 (8) (2003) 1194–1203, https://doi.org/10.1002/app.11452.
[10] S.M.R. Costa, D. Fowler, G.A. Carreira, I. Portugal, C.M. Silva, Production and upgrading of recovered carbon black from the pyrolysis of end-of-life tires, Materials (Basel, Switzerland) 15 (6) (2022) 2030, https://doi.org/10.3390/ma15062030.
[11] A.M. Cunliffe, P.T. Williams, Properties of chars and activated carbons derived from the pyrolysis of used Tyres, Environ. Technol. 19 (12) (1998) 1177–1190, https://doi.org/10.1080/09593331908616778.
[12] H. Darmstadt, C. Roy, S. Kaliaguine, Inorganic components and Sulphur compounds in carbon blacks from vacuum pyrolysis of used tires, Kautsch. Gummi Kunstst. 47 (1994) 891–895.
[13] H. Darmstadt, C. Roy, S. Kaliaguine, Characterization of pyrolytic carbon blacks from commercial tire pyrolysis plants, Carbon 33 (10) (1995) 1449–1455, https://doi.org/10.1016/0008-6223(95)00096-V.
[14] R.N. Datta, A review on heat and reversion resistance compounding, Progr. Rubb. Plast. Recycl. Technol. 19 (3) (2003) 143–170, https://doi.org/10.1177/147776060301900302.
[15] J.-B. Donnet, Fifty years of research and progress on carbon black, Carbon 32 (7) (1994) 1305–1310, https://doi.org/10.1016/0008-6223(94)90116-3.
[16] M. Ducousso, E. Weiss-Hortala, A. Nzihou, M.J. Castaldi, Reactivity enhancement of gasification biochars for catalytic applications, Fuel 159 (2015) 491–499, https://doi.org/10.1016/j.fuel.2015.06.100.
[17] P. Düngen, R. Schlögl, S. Heumann, Non-linear thermogravimetric mass spectrometry of carbon materials providing direct speciation separation of oxygen functional groups, Carbon 130 (2018) 614–622, https://doi.org/10.1016/j.carbon.2018.01.047.
[18] D. Eagland, The influence of hydration on the stability of hydrophobic colloidal systems, in: F. Franks (Ed.), Water in Disperse Systems, Springer US, 1975, pp. 1–74, https://doi.org/10.1007/978-1-4757-6961-6_1.
[19] K. Formela, A. Hejna, Ł. Zedler, X. Colom, J. Cañavate, Microwave treatment in waste rubber recycling – recent advances and limitations, Express Polym Lett 13 (2019) 565–588, https://doi.org/10.3144/expresspolymlett.2019.48.
[20] M. Göckeler, C.M. Berger, M. Purcel, R. Bergsträßer, A.-P. Schinkel, M. Muhler, Surface reactions during temperature-programmed desorption and reduction

experiments with oxygen-functionalized carbon blacks, Appl. Surf. Sci. 561 (2021) 150044, https://doi.org/10.1016/j.apsusc.2021.150044.
[21] U. Goerl, A. Hunsche, A. Mueller, H.G. Koban, Investigations into the silica/Silane reaction system, Rubber Chem. Technol. 70 (4) (1997) 608–623, https://doi.org/10.5254/1.3538447.
[22] A.P. Gregory, R.N. Clarke, Traceable measurements of the static permittivity of dielectric reference liquids over the temperature range 5–50 °C, Meas. Sci. Technol. 16 (7) (2005) 1506, https://doi.org/10.1088/0957-0233/16/7/013.
[23] K.S. Howard, R.A. McAllister, Surface tension of acetone-water solutions up to their normal boiling points, AICHE J. 3 (3) (1957) 325–329, https://doi.org/10.1002/aic.690030308.
[24] H. Huang, L. Tang, Pyrolysis treatment of waste tire powder in a capacitively coupled RF plasma reactor, Energy Convers. Manag. 50 (3) (2009) 611–617, https://doi.org/10.1016/j.enconman.2008.10.023.
[25] H. Kahl, T. Wadewitz, J. Winkelmann, Surface tension and interfacial tension of binary organic liquid mixtures, J. Chem. Eng. Data 48 (6) (2003) 1500–1507, https://doi.org/10.1021/je034062r.
[26] U. Kalitko, Waste Tire pyrolysis recycling with steaming: Heat-Mass Balances & Engineering Solutions for by-products quality, in: Material Recycling—Trends and Perspectives, IntechOpen, 2012, https://doi.org/10.5772/31535.
[27] V. Kalitko, Steam-thermal recycling of tire shreds: calculation of the rate of explosion-proof feed of steam, J. Eng. Phys. Thermophys. 81 (2008) 781–786, https://doi.org/10.1007/s10891-008-0092-6.
[28] W. Kaminsky, C. Mennerich, Pyrolysis of synthetic tire rubber in a fluidised-bed reactor to yield 1,3-butadiene, styrene and carbon black, J. Anal. Appl. Pyrolysis Complete (58–59) (2001) 803–811, https://doi.org/10.1016/S0165-2370(00)00129-7.
[29] I.S. Khattab, F. Bandarkar, M.A.A. Fakhree, A. Jouyban, Density, viscosity, and surface tension of water+ethanol mixtures from 293 to 323K, Korean J. Chem. Eng. 29 (6) (2012) 812–817, https://doi.org/10.1007/s11814-011-0239-6.
[30] R. Kitamura, L. Pilon, M. Jonasz, Optical constants of silica glass from extreme ultraviolet to far infrared at near room temperature, Appl. Opt. 46 (33) (2007) 8118–8133, https://doi.org/10.1364/AO.46.008118.
[31] M. Labaki, M. Jeguirim, Thermochemical conversion of waste tyres-a review, Environ. Sci. Pollut. Res. Int. 24 (11) (2017) 9962–9992, https://doi.org/10.1007/s11356-016-7780-0.
[32] W.M. Lewandowski, K. Januszewicz, W. Kosakowski, Efficiency and proportions of waste Tyre pyrolysis products depending on the reactor type—A review, J. Anal. Appl. Pyrolysis 140 (2019) 25–53, https://doi.org/10.1016/j.jaap.2019.03.018.
[33] N. Li, X. Ma, Q. Zha, K. Kim, Y. Chen, C. Song, Maximizing the number of oxygen-containing functional groups on activated carbon by using ammonium persulfate and improving the temperature-programmed desorption characterization of carbon surface chemistry, Carbon 49 (15) (2011) 5002–5013, https://doi.org/10.1016/j.carbon.2011.07.015.
[34] G. Lopez, M. Olazar, M. Amutio, R. Aguado, J. Bilbao, Influence of Tire formulation on the products of continuous pyrolysis in a conical spouted bed reactor, Energy Fuel 23 (11) (2009) 5423–5431, https://doi.org/10.1021/ef900582k.
[35] J.D. Martínez, N. Puy, R. Murillo, T. García, M.V. Navarro, A.M. Mastral, Waste Tyre pyrolysis – A review, Renew. Sust. Energ. Rev. 23 (2013) 179–213, https://doi.org/10.1016/j.rser.2013.02.038.
[36] J.D. Martínez, N. Cardona-Uribe, R. Murillo, T. García, J.M. López, Carbon black recovery from waste tire pyrolysis by demineralization: production and application in rubber compounding, Waste Manag. 85 (2019) 574–584, https://doi.org/10.1016/j.wasman.2019.01.016.
[37] S. Mostoni, P. Milana, M. D'Arienzo, S. Dirè, E. Callone, C. Cepek, S. Rubini, A. Farooq, C. Canevali, B. Di Credico, R. Scotti, Studying stearic acid interaction with ZnO/SiO2 nanoparticles with tailored morphology and surface features: A benchmark for better designing efficient ZnO-based curing activators, Ceram. Int. 49 (14, Part B) (2023) 24312–24321, https://doi.org/10.1016/j.ceramint.2022.12.013.
[38] L. Moulin, S. Da Silva, A. Bounaceur, M. Herblot, Y. Soudais, Assessment of recovered carbon black obtained by waste tires steam water Thermolysis: an industrial application, Waste Biomass Valoriz. 8 (2017), https://doi.org/10.1007/s12649-016-9822-8.
[39] P.K. Mubari, T. Beguerie, M. Monthioux, E. Weiss-Hortala, A. Nzihou, P. Puech, The X-ray, Raman and TEM signatures of cellulose-derived carbons explained, C 8 (1) (2022), https://doi.org/10.3390/c8010004. Article 1.
[40] H. Peter Bennetto, F. Evans, G., & J. Sheppard, R., Dielectric properties and structure of N -methylpropionamide + methanol mixtures, J. Chem. Soc., Faraday Trans. 1 79 (1) (1983) 245–251, https://doi.org/10.1039/F19837900245.
[41] J. Pikunic, P. Llewellyn, R. Pellenq, K.E. Gubbins, Argon and nitrogen adsorption in disordered nanoporous carbons: simulation and experiment, Langmuir 21 (10) (2005) 4431–4440, https://doi.org/10.1021/la047165w.
[42] M. Porter, T.D. Skinner, M.A. Wheelans, Structural characterization of vulcanizates. Part VIII. The N-cyclohexylbenzothiazole-2-sulfenamide-accelerated sulfur vulcanization of natural rubber at 140–180°C. and of synthetic cis-1,4-polyisoprene at 140°C, J. Appl. Polym. Sci. 11 (11) (1967) 2271–2283, https://doi.org/10.1002/app.1967.070111114.
[43] C. Presser, J.G. Radney, M.L. Jordan, A. Nazarian, Simultaneous transmission and absorption photometry of carbon-black absorption from drop-cast particle-laden filters, Aerosol. Sci. Technol.: J. Am. Assoc. Aerosol. Res. 53 (2019), https://doi.org/10.1080/02786826.2019.1577950.
[44] P. Puech, A. Dabrowska, N. Ratel-Ramond, G.L. Vignoles, M. Monthioux, New insight on carbonisation and graphitisation mechanisms as obtained from a bottom-up analytical approach of X-ray diffraction patterns, Carbon 147 (2019) 602–611, https://doi.org/10.1016/j.carbon.2019.03.013.
[45] N. Rattanasom, T. Saowapark, C. Deeprasertkul, Reinforcement of natural rubber with silica/carbon black hybrid filler, Polym. Test. 26 (3) (2007) 369–377, https://doi.org/10.1016/j.polymertesting.2006.12.003.
[46] C. Roy, H. Darmstadt, B. Benallal, C. Amen-Chen, Characterization of naphtha and carbon black obtained by vacuum pyrolysis of polyisoprene rubber, Fuel Process. Technol. 50 (1) (1997) 87–103, https://doi.org/10.1016/S0378-3820(96)01044-2.
[47] C. Roy, A. Chaala, H. Darmstadt, The vacuum pyrolysis of used tires: end-uses for oil and carbon black products, J. Anal. Appl. Pyrolysis 51 (1) (1999) 201–221, https://doi.org/10.1016/S0165-2370(99)00017-0.
[48] W. Ruland, B. Smarsly, X-ray scattering of non-graphitic carbon: an improved method of evaluation, J. Appl. Crystallogr. 35 (5) (2002) 624–633, https://doi.org/10.1107/S0021889802011007.
[49] A.B. Samsuri, in: S. Thomas, C. Han Chan, L. Pothen, J. Joy, H. Maria (Eds.), CHAPTER 3. Theory and Mechanisms of Filler Reinforcement in Natural Rubber Vol. 2, Royal Society of Chemistry, 2013, pp. 73–111, https://doi.org/10.1039/9781849737654-00073.
[50] V. Shulman, Tyre recycling, in: Waste, 2011, pp. 297–320, https://doi.org/10.1016/B978-0-12-381475-3.10021-X.
[51] K.S.W. Sing, F. Rouquerol, J. Rouquerol, P. Llewellyn, 8—Assessment of Mesoporosity, in: F. Rouquerol, J. Rouquerol, K.S.W. Sing, P. Llewellyn, G. Maurin (Eds.), Adsorption by Powders and Porous Solids, Second edition, Academic Press, 2014, pp. 269–302, https://doi.org/10.1016/B978-0-08-097035-6.00008-5.
[52] G.S. Szymański, Z. Karpiński, S. Biniak, Świątkowski, A., The effect of the gradual thermal decomposition of surface oxygen species on the chemical and catalytic properties of oxidized activated carbon, Carbon 40 (14) (2002) 2627–2639, https://doi.org/10.1016/S0008-6223(02)00188-4.
[53] A.G. Talma, R.N. Datta, N.M. Huntink, P.G.J. Nieuwenhuis, Hardness stabilization in rubber vulcanizates (European Union Patent EP1072640A1). https://patents.google.com/patent/EP1072640A1/en, 2001.
[54] M. Thommes, K. Kaneko, A.V. Neimark, J.P. Olivier, F. Rodriguez-Reinoso, J. Rouquerol, K.S.W. Sing, Physisorption of gases, with special reference to the evaluation of surface area and pore size distribution (IUPAC technical report), Pure Appl. Chem. 87 (9–10) (2015) 1051–1069, https://doi.org/10.1515/pac-2014-1117.
[55] D. Torani, J. da S. Crespo, R.N. Brandalise, Influence of ZnO on the properties of elastomeric compositions and their leached extract, Polímeros 29 (2019) e2019041, https://doi.org/10.1590/0104-1428.07218.
[56] N.B. Vargaftik, B.N. Volkov, L.D. Voljak, International tables of the surface tension of water, J. Phys. Chem. Ref. Data Monogr. 12 (3) (1983) 817–820, https://doi.org/10.1063/1.555688.
[57] P.T. Williams, Pyrolysis of waste tyres: A review, Waste Manage. (New York, N.Y.) 33 (8) (2013) 1714–1728, https://doi.org/10.1016/j.wasman.2013.05.003.
[58] P.T. Williams, S. Besler, Pyrolysis-thermogravimetric analysis of tyres and Tyre components, Fuel 74 (9) (1995) 1277–1283, https://doi.org/10.1016/0016-2361(95)00083-H.
[59] M.A. Wojtowicz, M.A. Serio, Pyrolysis of scrap tires: can it be profitable? ChemTech 26 (10) (1996). https://www.osti.gov/biblio/404473.
[60] Jeffries Wyman, The dielectric constant of mixtures of ethyl alcohol and water from −5 to 40°, J. Am. Chem. Soc. 53 (9) (1931) 3292–3301, https://doi.org/10.1021/ja01360a012.
[61] S.T. Yang, M.J. Matthews, S. Elhadj, D. Cooke, G.M. Guss, V.G. Draggoo, P. J. Wegner, Comparing the use of mid-infrared versus far-infrared lasers for mitigating damage growth on fused silica, Appl. Opt. 49 (14) (2010) 2606–2616, https://doi.org/10.1364/AO.49.002606.
[62] J. Yu, J. Xu, Z. Li, W. He, J. Huang, J. Xu, G. Li, Upgrading pyrolytic carbon-blacks (CBp) from end-of-life tires: characteristics and modification methodologies, Front. Environ. Sci. Eng. 14 (2) (2019) 19, https://doi.org/10.1007/s11783-019-1198-0.
[63] S. Yurdakal, C. Garlisi, L. Özcan, M. Bellardita, G. Palmisano, Chapter 4 - (photo) catalyst characterization techniques: Adsorption isotherms and BET, SEM, FTIR, UV–vis, photoluminescence, and electrochemical characterizations, in: G. Marcì, L. Palmisano (Eds.), Heterogeneous Photocatalysis, Elsevier, 2019, pp. 87–152, https://doi.org/10.1016/B978-0-444-64015-4.00004-3.
[64] R. Zafarmehrabian, S.T. Gangali, M.H.R. Ghoreishy, M. Davallu, The effects of silica/carbon black ratio on the dynamic properties of the tread compounds in truck tires, E-J. Chem. 9 (3) (2012) 1102–1112, https://doi.org/10.1155/2012/571957.
[65] G. Zhang, Y. Jiang, S. Wang, Y. Zhang, Influence of a novel coupling agent on the performance of recovered carbon black filled natural rubber, Compos. Part B Eng. 255 (2023) 110614, https://doi.org/10.1016/j.compositesb.2023.110614.
[66] J.-H. Zhou, Z.-J. Sui, J. Zhu, P. Li, D. Chen, Y.-C. Dai, W.-K. Yuan, Characterization of surface oxygen complexes on carbon nanofibers by TPD, XPS and FT-IR, Carbon 45 (4) (2007) 785–796, https://doi.org/10.1016/j.carbon.2006.11.019.